ELSEVIER

Nuclear Instruments and Methods in Physics Research A 404 (1998) 295–304

NUCLEAR INSTRUMENTS & METHODS IN PHYSICS RESEARCH Section A

Central tracking chamber with inflated cathode-strip foils

E.W. Blackmore[a], D.A. Bryman[a,*], Y. Kuno[a,1], C. Lim[a], T. Numao[a], P. Padley[a,2], G. Redlinger[a], R. Soluk[a], R.A. McPherson[b,3]

[a] *TRIUMF, 4004 Wesbrook Mall, Vancouver, BC, Canada, V6T 2A3*
[b] *Joseph Henry Laboratories, Princeton University, Princeton, NJ 08544, USA*

Received 22 August 1996; received in revised form 23 September 1997

Abstract

A new cylindrical low-mass central drift chamber has been constructed for the $K^+ \to \pi^+ \nu\bar{\nu}$ experiment at BNL (E787). The chamber consists of twelve layers of axial wire cells and six layers of thin cathode-strip foils, four of which are supported by differential gas pressure. The momentum resolution (RMS) for muons and pions in the range 150–250 MeV/c is found to be about 0.9%.

Keywords: Drift chamber; Cathode strips

1. Introduction

A measurement of the rare decay $K^+ \to \pi^+ \nu\bar{\nu}$, predicted in the Standard Model (SM) to occur with a branching ratio around 10^{-10} [1], is in progress at Brookhaven National Laboratory (E787) [2]. $K^+ \to \pi^+ \nu\bar{\nu}$ is a unique reaction for examining the detailed predictions of higher-order effects in the SM and measurement of the branching ratio is expected to lead to a clean determination of the quark-mixing parameter V_{td}. Recently, E787 has been upgraded to gain an order-of-magnitude in sensitivity.

Among the goals of the upgrade was a significant improvement in the momentum measurement (performed in a 1 T magnetic field) to enhance the particle identification capability of the detector and reduce backgrounds associated with $K^+ \to \mu^+ \nu$ ($K_{\mu 2}$), $K^+ \to \mu^+ \nu\gamma$ and $K^+ \to \pi^+ \pi^0$ ($K_{\pi 2}$) decays. The momentum resolution of the original E787 chamber [3] was 2.4% (RMS) for pions and muons in the range 150–250 MeV/c (including a 0.9% contribution from energy lost in the kaon stopping target). Since the momentum resolution was limited primarily by multiple Coulomb scattering, a substantially lower mass chamber was required. This objective was realized by incorporating a novel design using thin, internally inflated cathode strip foils.

The new chamber is a cylinder of length 51 cm and radius 43 cm, as illustrated in Fig. 1. To

* Corresponding author. Tel.: + 1 604 222 1047; fax: + 1 604 222 1074; e-mail: bryman@triumf.ca.

[1] Present address: Physics Department, National Laboratory for High Energy Physics (KEK), Tsukuba, Ibaraki 305, Japan.

[2] Present address: T.W. Bonner Nuclear Laboratory, Rice University, Houston, TX 77005.

[3] Present address: European Laboratory for Particle Physics (CERN), CH-1211 Geneva 23, Switzerland.

0168-9002/98/$19.00
PII S0168-9002(97)01163-7

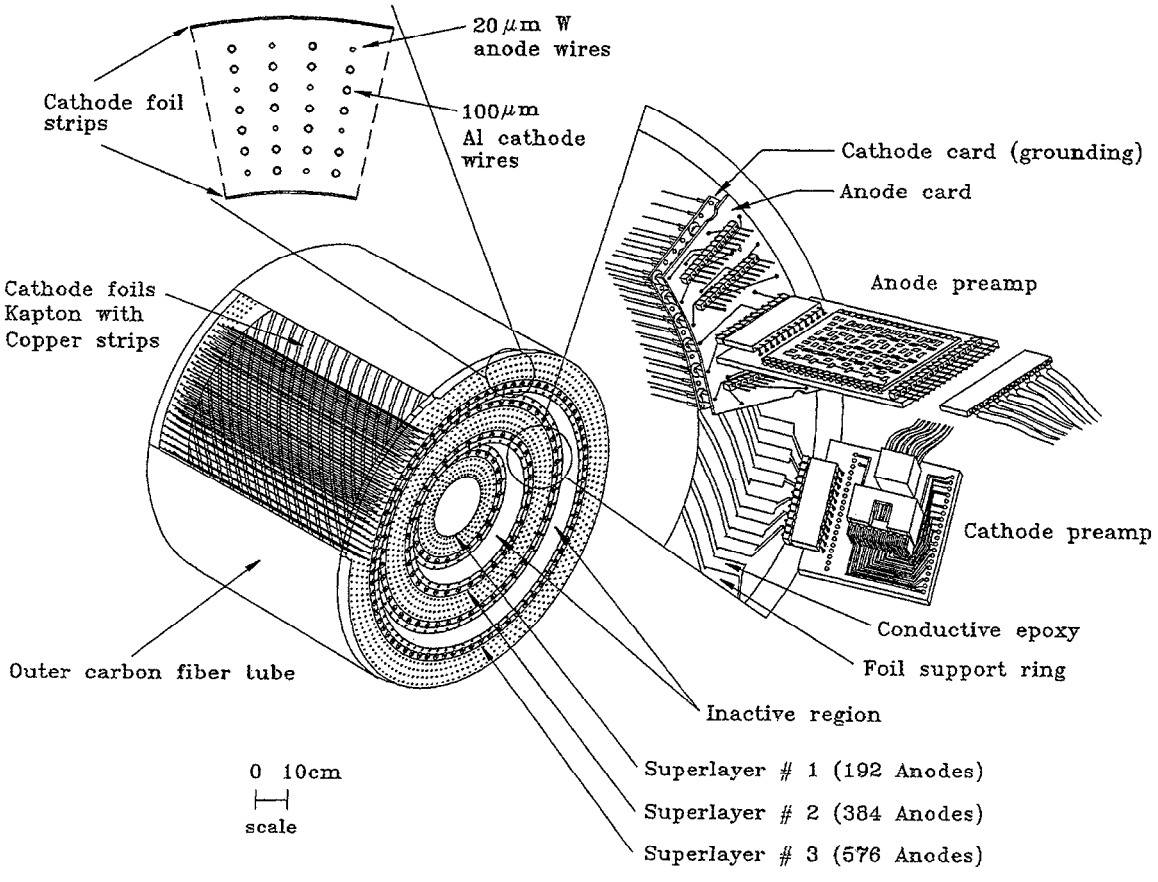

Fig. 1. Schematic of the new E787 central drift chamber.

measure the xy position coordinates perpendicular to the chamber axis (z), three superlayers of axial sense wires are arranged in square cells. Each superlayer has four layers of cells for which the active chamber gas is contained between two thin cathode foils supported by differential gas pressure. The foils have metalized strips for induced charge measurement to obtain the longitudinal (z) coordinates. Thus, track coordinate information typically consists of twelve xy measurements and six z points.

Previously, "balloon" chambers with single-layer cylindrical multi-wire proportional chambers (MWPC) have been constructed for the CPLEAR [4] experiment at CERN and the MEGA [5] experiment at LAMPF. Many other cylindrical central drift chambers (e.g. see Ref. [6]) have used cathode strips or pads at the innermost and outer radii adjacent to support tubes as a part of the z-coordinate measurement. For the central drift chamber geometry described here, the advantages of the balloon foil arrangement for all superlayers include low mass, all-axial wire construction and redundant high precision z-coordinate measurements throughout the measurement volume (with reduced dependence on the xy measurements as in stereo wire arrangements).

In the following, the design and performance of the E787 central drift chamber will be discussed.

2. Chamber design

To minimize mass in the detection region, aluminum cathode wires were used and the inactive

chamber regions between superlayers (see Fig. 1) were filled with nitrogen gas[4]. Compared to the previous chamber, a 15% longer measurement path length (totalling about 35 cm) was achieved by reducing the innermost radius of the chamber to the minimum possible and by switching from a jet-cell chamber to a square-cell design.

The new chamber consists of three active cylindrical superlayers, each with four layers of small square drift cells with sides of 11–19 mm, and two inactive volumes with a thickness of ~ 9 cm between the superlayers. A square-cell geometry was chosen in order to match the use of cathode-strip foils at the inner and outer radii of each superlayer. A cell (shown in Fig. 1.) consists of one 20 μm diameter gold-plated tungsten sense wire surrounded by eight 100 μm gold-plated aluminum cathode wires at the four corners of a "square" and at the middle of each "side". Cathode wires are shared with the adjacent cells. Every other layer is shifted by one-half cell to allow a local resolution of left–right ambiguity. The cathode wires are grounded and the anode wires are connected via decoupling capacitors on the downstream end to printed circuit (PC) cards on which the preamplifiers are mounted. The high voltage distribution to the anode layers is on the upstream end.

Instead of cathode wires, each radial end of a superlayer has a 25 μm thick Kapton foil with 1200 Å thick 7 mm wide copper strips (coated with 300 Å nickel) tilted at 45° with respect to the z-axis and with a 1 mm gap between strips. The foils provide z-coordinate measurements for each track (via measurement of the induced charge on the strips) and also serve to separate the active and inactive gas volumes.

Surface fields for operational conditions were calculated to be 260 kV/cm for the sense wires, < 15 kV/cm for the cathode wires and < 1 kV/cm for the foils. The gas gain for a 50 : 50 mixture of argon–ethane is about 8×10^4. The overall mass in the measurement region (excluding the inner and outer support tubes as well as the innermost and outermost foils) amounts to 2×10^{-3} radiation lengths. This represents a reduction in mass of about a factor of 4 compared to the previous E787 chamber described in Ref. [3].

For this design, Monte Carlo calculations predicted a momentum resolution $\Delta P = 2.3$ MeV/c (RMS) for π^+ from the decay $K^+ \to \pi^+\pi^0$ at 205 MeV/c (or $\Delta P/P$ of 1.1%), assuming position resolutions $\sigma_{xy} = 150$ μm and $\sigma_z = 1$ mm. The estimated momentum resolution included a contribution from uncertainty in the correction for pion energy loss in the kaon stopping target; this uncertainty amounted to $\Delta P = 1.8$ MeV/c, independent of momentum.

A summary of the chamber parameters is given in Table 1.

3. Construction

The inner support tube with inside diameter 157 mm was made from 0.38 mm thick G10 (density ~ 1.7 g/cm^3) epoxied at each end to an aluminum ring. The outer support cylinder with outside diameter of 866 mm and effective thickness of 82.5 mg/cm^2 was made from four layers of preimpregnated carbon fiber arranged at angles of 45°, 0°,0° and $-45°$. To ease the stringing of the chamber and to permit replacement of the cathode foils, the three concentric end plates were arranged in a nested structure separated and supported by conical-shaped aluminum rings on either side of the middle superlayer. The end plates can be held apart by sets of removable aluminum expansion rods and can be pre-loaded by means of similar compression rods with springs at the same four radii. The wires were located to a precision of about 50 μm using crimp pins[5] pressed into holes drilled with a numerically controlled machine into the plastic annular endplates.

The sense wires were tensioned at 40 g, the field wires at 100 g and the cathode foils at 40 g/cm giving a total endplate loading of 360 kg. A combination of calculations and loading tests of

[4] Further reduction in mass could be achieved by using helium-based gases [7–10] in all regions of the chamber, but for the present purposes, the relative improvement in performance was not substantial.

[5] Size A1, manufactured by Medelec, Puidoux, CH-1604 Switzerland.

Table 1
Chamber parameters

Sense wires	1152 cells in twelve layers, grouped in three superlayers
	Number of cells per layer in a superlayer: 48, 96, 144
	20 μm gold-plated tungsten (tension: 40 g)
Cathode wires	100 μm gold-plated aluminum (tension: 100 g)
Foils	Number of layers: 6
	Number of strips per foil: 48, 72, 108, 144, 180, 216
	Active length in z (cm): 38.8, 38.8, 44.8, 44.8, 50.8, 50.8
	25 μm Kapton plus 1200 Å copper, 300 Å nickel (tension: 40 g/cm)
Inner cylinder	Inner radius: 7.85 cm, Length: 38.8 cm
	0.038 cm thick G10
Outer cylinder	Outer radius: 43.31 cm, Length: 50.8 cm
	four layers preimpregnated carbon fiber
	Thickness: 0.1 cm (effective thickness 82.5 mg/cm^2)
Outer cylinder spacer	Inner radius: 42.81 cm
	0.4 cm thick Rohacell (effective thickness 24 mg/cm^2)
End plates	1.20cm thick ULTEM (inner superlayer)
	1.20 cm thick NORYL (middle and outer superlayers)
	0.40 cm thick aluminum (intermediate support)
Gas	Active volume: argon–ethane–ethanol (49.6% : 49.6% : 0.8%)
	Inactive regions: nitrogen
	Gain: 8×10^4
	Drift velocity: 5 cm/μs
Voltages	Anodes: + 2 kV
	Cathodes: ground
Surface fields	Anodes: 260 k/cm
	Cathodes: < 15kV/cm
	Foils: < 1 kV/cm

simulated structures was used to determine the endplate thickness and support arrangement to maintain deflections during stringing to acceptable levels. ULTEM[6] which has a flexural modulus of 3.3×10^3 MPa was selected for the inner layer end plate which has the highest linear loading. NORYL[7] was used for the middle and outer layers. The plastic end plates are 12 mm thick and the aluminum conical rings which provide the intermediate support are 4 mm thick.

The pattern of strips was etched onto the cathode foils, the largest of which measured 75 cm × 385 cm, using a positive photoresist process. The mask was prepared by first drawing a negative image of the pattern on a mylar sheet on a large flat-bed plotter, then transferring the image to a sheet of ultraviolet-sensitive contact film in order to get the best contrast. A foil loop of the correct circumference was then made using an adjustable mandrell, and the foils were epoxied to end rings spaced apart by the expansion rods to the correct distance to produce the desired tension on the foils when they were mounted on the chamber. The inner foil was mounted on the outside of the G10 inner cyclinder and the outer foil was spaced 4 mm from the outer graphite support cylinder (which is conducting) by a layer of Rohacell[8]. The effective thickness of the Rohacell layer was 24 mg/cm^2. Silver epoxy paste

[6] ULTEM is a polyetherimide manufactured by General Electric Company.

[7] NORYL is a polyphenylene ether blended with polystyrene, manufactured by General Electric Company.

[8] Rohacell is a rigid plastic foam, chemically a polymethacrylimide, available from Rohm Tech Inc. in Malden, Maine. Different densities are available to optimize strength/mass. The Rohacell used in this chamber had a density of 61.5 mg/cm^3.

was used to make the electrical connections between the foil and copper strips to which the pre-amplifier connectors were soldered.

Thin mylar strips coated with weak Fe^{55} sources were mounted on the inside of the end plates, providing counting rates of a few hundred Hz on all channels for diagnostic purposes.

A 50 : 50 argon/ethane mixture was delivered to the three active regions and nitrogen to the intermediate superlayers. The argon was bubbled through ethanol at 0°C. A differential pressure of about 2 cm H_2O was provided across each of the four inner cathode foils to keep the foils stretched. The exhaust gas from each superlayer was bubbled through tubes immersed at different depths in a mineral oil ($C_{16}H_{22}O_4$) bath in order to maintain the relative pressures between superlayers. The depths increased monotonically from about 1 cm for the outermost foil to about 15 cm for the innermost foil.

4. Electronics

Electrical connections to the anode (signal) and cathode (ground) wires were made by means of mating sockets soldered into PC cards which had the same hole pattern as the anode/cathode wires in the end plates. Superlayers 1, 2 and 3 were subdivided (for ease of construction) into 8, 16 and 12 sectors, respectively, for grounding and readout. All cathode wires were grounded by PC cards on the downstream endplate (each card covers one sector) to the common ground, i.e. the aluminum conical end plates and the inner and outer cylinders. The cathode cards had holes in the positions of the anode wires, allowing anode cards to be mounted on top of them. The pre-amplifiers were mounted on these anode cards and connected to the sense wires via 4 kV, 1820 pF decoupling capacitors. Cathode strips were connected through etched strips on a thin G10 ring to a 12-pin connector on which cathode pre-amplifiers were mounted. Because of radial space limitations, the outputs of the outermost foil were connected by a flexible ribbon cable to the adjacent anode card where the pre-amplifier was mounted.

The pre-amplifier and the post-amplifier were linked by a series of two 50 Ω coaxial cables: an eight-cable bundle of 3–5 m long miniature ALPHA 9374 cables between the pre-amplifier and a bulkhead, and 30 m long RG174 cables to the post-amplifiers, located in the counting house. The pre-amplifiers and postamplifier-discriminators were of the same design as that of the previous chamber [3] with slight modifications. Both anode and cathode pre-amplifier cards contained six amplifiers based on a common-base input BFT25 transistor. The differences from the previous system include the removal of a cross-talk cancellation network (which was required in the previous geometry due to close proximity of the anode wires in the "jet cell" [3]) and reversal of polarity at the input of the cathode post-amplifier. In order to approximately balance the pulse height in the analog outputs of anodes and cathodes, the gain of the cathode analog path was set to be larger than the anode by a factor of 5. The pre-amplifier gains were 5 and 10 mV/μA for the anodes and cathodes, respectively. The corresponding post-amplifier gains were 10 and 25. Total charge on each anode wire and cathode strip was measured by a Lecroy 1881 ADC; time was measured by a Lecroy Fastbus 1879 TDC fed by a discriminator with ECL output on the postamp board.

A separate high voltage was fed to each semicircular half of a layer; it was brought in from a bulkhead on a single-wire HV cable (Gore F01A030), filtered at the anode card on the downstream end plate and fed to a single-anode wire. This anode wire was then connected on the upstream end plate to a bus line through a 100 kΩ resistor. The bus line was connected to each of the remaining anode wires in that half of the layer through a 1 MΩ resistor.

5. Track finding/fitting

Track finding/fitting was performed separately for the xy and z views. For simplicity, tracks were fit to a circle in the xy-plane and separately to a straight line in the "xy turning angle" versus z plane, rather than a simultaneous helix fit.

In xy, drift times were corrected for pedestals and then converted into drift distances, defined as the distance of closest approach to the sense wire. The time–distance relation was parametrized separately for each layer using a 6th-order polynomial. Corrections were applied as a function of the track incidence angle (relative to the radial direction) for the left and right[9] sides of the cell in order to take into account the deviations of the isochrones from circles; the correction was determined in track angle bins and was applied with quadratic interpolation. The application of the correction was an iterative process, using the current best estimate of the track parameters.

Track candidates were identified as follows. For each superlayer, hit wires were grouped into clusters based on their spatial proximity to one another. Each cluster was reduced to a vector by a crude straight-line fit to the hits, assuming azimuthal drift and weighting all hits equally. Left–right ambiguities could be resolved for most cases by taking the fit with the best χ^2. Vectors were then linked, based on the angle between each of the two vectors and the line connecting them [11,12]. Starting parameters for the track were estimated by a circle fit [13] to space points for the linked wires; for the purposes of this estimation, the space points were determined by assuming azimuthal drift and using the left–right assignments from the vector fitting stage. Tracks were fit using an algorithm developed for MARK II [14,15] which combined track fitting to drift circles with the ability to refine the left–right assignments based on a global χ^2. Outlying hits were removed by an iterative procedure. Hits with fit residuals (i.e. differences between fitted and measured positions), scaled by expected resolution, greater than a gradually tightening threshold were removed one by one, starting with the worst offender, and refitting the track after each hit was removed. After each iteration, unused hits with scaled residuals less than a gradually tightening threshold were added to the track. Tracks with eight or more hits were accepted for further analysis.

[9] Left and right are defined by the sense of the cross product between the radial vector and the direction of the magnetic field.

In z, strips with ADC values above pedestal by more than 3 times the RMS of the pedestal distribution were grouped into clusters. The ADC values for each strip were corrected for pedestal and gain. Clusters were assigned to xy tracks if the strips crossed the wires on the track in the adjacent layer; clusters were allowed to be assigned to more than one track, and more than one cluster could be assigned to a track per foil at this stage. Each cluster-wire crossing was assigned a z position by taking the ADC-weighted mean of the strip-wire crossing points. An empirical correction to the z position was then applied as a function of the distance between the centroid and the midpoint of the cluster of hit strips.

At typical beam rates (8×10^5 K^+ stops/s), most tracks had more than one cluster initially assigned per foil. All pairs of clusters that were greater than two foils apart were selected and a straight-line fit through each pair (in the "xy turning angle" versus z plane). Each line was then extrapolated to the foils and the closest hit within a certain distance of the line was added to the set of candidate hits; the "road width" was based on an estimate of the track extrapolation error plus a constant hit resolution term. The set of hits with the smallest χ^2 per degree of freedom was taken as the track candidate. This χ^2 was constructed from the sum of two parts: an "ADC" part where the χ^2 contribution was the z residual divided by the expected resolution, and a "TDC" part where each foil hit with a TDC time within a window of the wire time in the adjacent layer was assigned a χ^2/d.o.f. of 1.

6. Calibration and position resolution

6.1. Time–distance calibration

The first stage in the xy calibration was the determination of the timing pedestal (or t_0, i.e. "zero" time or drift distance) for each anode and cathode channel. This was done by a fit of the edge of the timing distribution to a convolution of a step function with a Gaussian, or error function. Taking the half-height of the step as the pedestal, this allowed all channels to be aligned relative to one another. The time–distance relation allowed a more

precise global offset from the track fit to be applied later.

The time–distance relation with the magnetic field off was established by an iterative procedure, using $K_{\mu 2}$ data. Starting with a linear time–distance relationship, using the estimated drift velocity for argon/ethane, straight-line fits were made to track segments within a single superlayer and average residuals measured as a function of drift time. These values were used to correct the time–distance relation; tracks were refit, and the procedure repeated until convergence was achieved. For data with no magnetic field, it was sufficient to find one time–distance relation per layer.

After aligning the superlayers (see below), the time–distance relation in a $B = 1$ T magnetic field was determined with tracks fit to all three superlayers. Starting with the time–distance relation for $B = 0$, the average value of the residuals as a function of drift time were used to obtain the time–distance relation for the next iteration. The time–distance relation was parametrized as a sixth-order polynomial and was a function of layer, incident angle of the track and left/right side of the cell. An example of the time–distance relations for layer four, which has a foil on the outer radial cell boundary, is shown in Fig. 2. Near the sense wire, the electric field dominates and the drift paths are almost radial with respect to the sense wire. For larger drift times, an asymmetry due to the Lorentz force distorts the drift paths from being purely radial. The large overall splitting between the left and right sides of the cell is due to the presence of a cathode foil on one of the cell boundaries. In the case of the layer shown in the figure, charge drifting from the right side of the cell travels through a longer path than charge from the left resulting in a longer drift time for the same distance of closest approach to the sense wire.

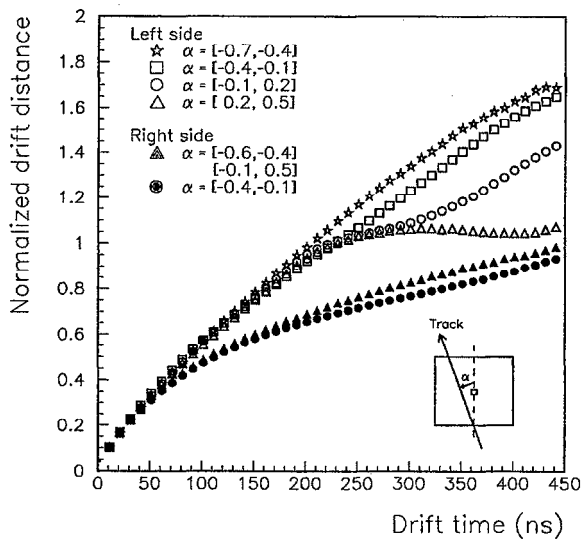

Fig. 2. Normalized drift distance versus time and angle for layer 4, which has a cathode foil on the outer radial cell boundary. Each symbol shows the drift distance versus time for a bin in track incidence angle (in radians), where the angle of the track (solid line in the inset diagram) is measured relative to the radial direction (dashed line in the inset). The magnetic field points out of the page in the inset. The normalized drift distance is the drift distance scaled by the half-width of the drift cell (0.83 cm); it can exceed 1 when the charge drifts from the corner of the cell.

6.2. *xy-position resolution*

The RMS of the xy residual distributions (fit to single Gaussian distributions) in the same layer as above are shown in Fig. 3 as a function of drift distance (scaled by the half-width of the cell) and track incidence angle. The maximum normalized drift distance cuts off at a different value as a function of incidence angle, reflecting the cutoff in maximum accepted drift time (see Fig. 2). The structure seen in the middle two plots for the left side of the cell at a normalized drift distance of about 1 results from the superposition of effects at different angles within the angle bin. For track incidence angles close to 0°, the resolution deteriorates near the edge of the cell at a maximum normalized drift distance of 1, whereas for larger angles, the resolution deteriorates at larger drift distances.

6.3. *z-position calibration*

The relative gains of the anode amplifiers/ADCs for each layer were determined with fitted tracks by lining up the peaks of the Landau distributions. An iterative procedure was necessary for the cathode chain. The highest ADC value of the strips in each cathode cluster was scaled by the gain-corrected ADC value of the anode wire hit in the adjacent

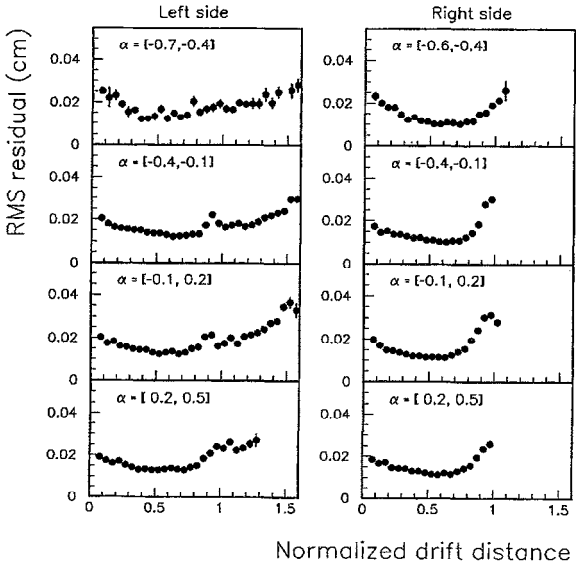

Fig. 3. RMS of the xy residuals in $K_{\mu 2}$ events (236 MeV/c) as a function of the normalized drift distance and track incidence angle, shown in layer 4 for the left and right sides of the cell. The "residual hit" was excluded from the track fit.

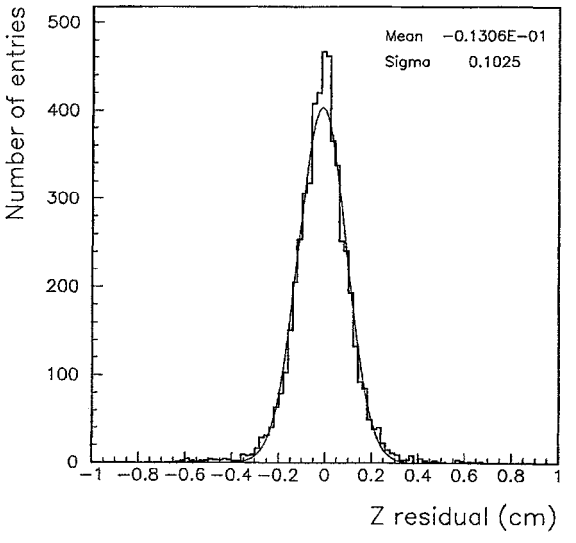

Fig. 4. z residuals in cosmic ray events, shown for the inner foil in the middle superlayer (adjacent to axial wire layer 5). The "residual hit" was excluded from the track fit.

layer. For each cathode channel, the peak of this (Gaussian) distribution was then used to estimate the gain. The procedure was then repeated until the gain factors converged (typically in three or four iterations). For both anodes and cathodes, the RMS spread in gain factors was found to be around 10%.

The z position of foil clusters was initially determined by the ADC-weighted mean of the crossing points between the strips in the cluster and the anode wire(s) hit in the adjacent layer. The average z residual as a function of the difference between the cluster centroid and the midpoint of the hit strips in the cluster was used to correct for a possible non-Gaussian charge distribution. These corrections (typically ~ 800 μm) were determined separately for each foil and as a function of the number of strips in the cluster.

6.4. z-position resolution

Typical z residuals in cosmic ray events, where the two branches have been fit to a single track, are shown in Fig. 4 for the inner foil on the middle superlayer. The z residual distribution is $\sim 20\%$ wider for the inner foil on the innermost superlayer where the signal to noise is worse due to larger foil capacitance to the ground potential of the central support tube.

6.5. Alignment

$K_{\mu 2}$ data with the magnetic field off were used to establish the relative alignment of the anode wires by superlayer. Each superlayer was treated as a rigid cylinder with three alignment parameters, two for translation perpendicular to the beam axis, and one for rotation about the beam axis. Straight tracks were fit to the hits in the middle superlayer, which was held fixed. These tracks were extrapolated to the other superlayers and the average residuals were used to estimate the alignment parameter relative to the middle superlayer. The three superlayers were found to be concentric to better than 90 μm; relative rotations between the superlayers were 0.3 and 0.7 mrad. The global alignment of the chamber in the xy plane relative to the rest of the detector was parametrized by a single rotation parameter about the beam axis. This parameter

was determined by lining up the drift chamber tracks with hits in a system of straw tube wire chambers situated inside the Range Stack [16].

Cosmic rays passing through the entire chamber with the magnetic field off (with typically 24 layers hit in xy and 12 foil hits in z) were used to calibrate the relative alignment of the foils. Each foil had one alignment parameter, corresponding to rotation[10] about the beam axis. The foil rotation parameters were adjusted until the z residuals were centered about 0. Rotation parameters ranged from -0.4 to 0.3 rad. The (relatively large) size of these corrections results from the choice of the initial foil settings. Although it was known that the foil positions were actually determined by the azimuthal positions of the preamps mounted on the foil support ring (see Fig. 1), the initial foil settings were simply chosen such that the strips were lined up with certain fiducial sense wires.

A first estimate of the global rotation of all the foils relative to the anode planes was determined by looking at the edges of the occupancy distribution of hit wire/strip concidences. A more precise determination was made by measuring the positions of the edges of fiducial scintillation counters whose distance from the magnet iron were well known.

The possibility of a coherent twist of all the superlayers was investigated with cosmic ray events. Such a twist, if it existed, would result in the two branches of the cosmic ray (where a branch denotes that part of the track in one half of the chamber) not being back-to-back in the xy plane, with a discrepancy proportional to $\Delta z/\Delta r$ between, for example, the two outermost points on the track. No evidence of a twist was found, at a level corresponding to a displacement at the outermost radius of less than 50 μm.

The angle of the cathode strips with respect to the beam axis was calibrated by examination of the linear dependence of the average z residual as a function of z, separately for each foil. The angles were adjusted iteratively until the z-dependence was removed. Typical adjustments were at the level of 0.4% in the tangent of the angle, corresponding to a z residual of about 1mm at the end of the foil.

[10] Note that a foil rotation gives rise to a shift in the reconstructed z position of the foil cluster.

7. Tracking performance

The anode efficiency was determined by selecting clusters in a superlayer with three or more layers hit, fitting a straight line to three of the layers using a crude drift model, then extrapolating to a cell in the remaining layer, and examining it for the presence of a hit. Typical operating voltages (about 2 kV) were 100–150 V above the edge of the voltage plateau, leading to efficiencies $> 99\%$ per layer.

The cathode hit reconstruction efficiency was determined by selecting tracks fit with three or more foil hits, then examining the remaining three foils for the presence of a cluster close to the track extrapolation point. Cathode efficiencies ranged from 98% to 99%.

The track reconstruction efficiency was determined from $K_{\mu 2}$ events (selected with loose cuts on the energy and range in the range stack) to be 100% at incident rates of $\sim 2 \times 10^5$ stopping kaons/s, dropping to 97% at the nominal intensity in the 1995 run of 8×10^5/s. The inefficiency was due to pattern recognition errors.

The momentum resolution obtained for $K_{\pi 2}$ and $K_{\mu 2}$ events is shown in Fig. 5. A fit to a single Gaussian leads to a total momentum resolution

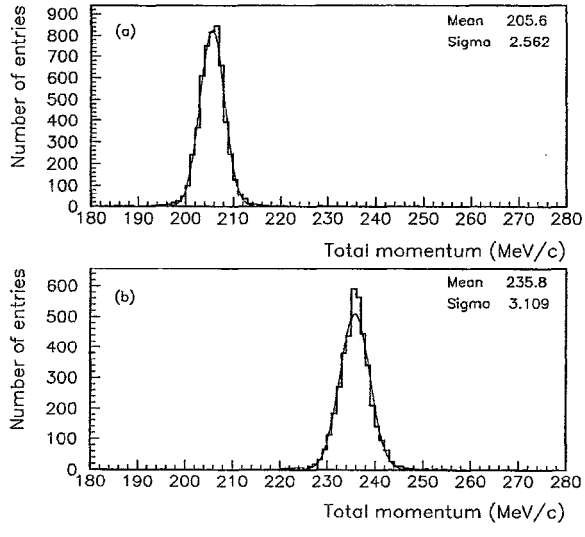

Fig. 5. Momentum distributions for (a) $K_{\pi 2}$ and (b) $K_{\mu 2}$ events, including corrections for energy lost in the target.

(RMS) of 1.3%. Removal in quadrature of the target contribution (estimated to be 1.8 MeV/c for $K_{\pi 2}$ events) would imply a chamber resolution component of 0.9%.

8. Summary

A low-mass central drift chamber with twelve layers of axial wire cells and six layers of thin cathode-strip foils, four of which are supported by differential gas pressure, has been constructed for experiment E787 at BNL. The chamber mass amounts to about 2×10^{-3} radiation lengths in the measurement region and about 3×10^{-2} radiation lengths overall, including inner- and outer-support tubes. The chamber provides a momentum measurement for muons and pions in the momentum range 150–250 MeV/c with an accuracy of 0.9%. This chamber is expected to play a major role in achieving the sensitivity required to measure the rare process $K^+ \to \pi^+ \nu\bar{\nu}$.

Acknowledgements

We are indebted to D. Marlow and others of our E787 colleagues for their encouragement. We also gratefully acknowledge the contributions of M. Goyette, R. Henderson, V. Kujala, D. Liu, R. Openshaw, V. Pacradouni and P. Vincent. This project was supported by the Natural Sciences Engineering Research Council and by TRIUMF.

References

[1] G. Buchalla, A. Buras, Nucl. Phys. B 412 (1994) 106.
[2] S. Adler et al., Phys. Rev. Lett. 76 (1996) 1421.
[3] J.V. Cresswell et al., IEEE Trans. Nucl. Sci. 35 (1985) 460.
[4] M. Dejardin et al., Nucl. Instr and Meth. A 283 (1989) 484.
[5] S. Stanislaus et al., Nucl. Instr and Meth. A 323 (1992) 198.
[6] D.G. Cassel et al., Nucl. Instr and Meth. A 252 (1986) 325.
[7] See, for example: S. Uno et al., Nucl. Instr. and Meth. A 320 (1993) 55.
[8] P.R. Burchat et al., Nucl. Instr and Meth. A 316 (1992) 217.
[9] V. Cindo et al., Nucl. Instr and Meth. A 309 (1991) 411.
[10] W. Zimmermann et al., Nucl. Instr and Meth. A 243 (1986) 86.
[11] M.D. Hildreth et al., IEEE Trans. Nucl. Sci. 42 (1995) 451.
[12] W.B. Atwood, SLD Detector Note 135, 31 October 1985.
[13] N. Chernov, G. Ososkov, Comp. Phys. Commun. 33 (1984) 329.
[14] M. Davies-White et al., Nucl. Instr and Meth. 160 (1979) 227.
[15] A. Johnson, G. Trilling, MARK II Internal Note TG-301, September 1978.
[16] M.S. Atiya et al., Nucl. Instr and Meth. A 321 (1992) 129.